A Model-Based Adaptive Control of Turning Maneuver for Catamaran Autonomous Surface Vessel

IGOR ASTROV, IRINA ASTROVA
Department of Software Science,
Tallinn University of Technology,
Akadeemia tee 15a, 12618, Tallinn,
ESTONIA

Abstract: - The effective computer control of airborne, waterborne, and ground autonomous vehicles has become one of the highest priorities in the area of cyber-physical systems, Industry 4.0 in particular, and the world economy in general. Despite extensive research on Unmanned Aerial Vehicles (UAVs), the study of Autonomous Surface Vessels (ASVs) has been more than ten times less intense. As an attempt to fill a gap in that field, this article discusses the control mathematics of a realistic ASV nonlinear model of a real autonomous electric catamaran "Nymo", which was designed at Tallinn University of Technology (TalTech). More technically, the article offers a novel adaptive control system that is based on knowledge of the main parameters of ASV and is specially designed for a Simulink/MATLAB environment. The article also enables adjusting variables like transition time and heading angle overshoot value. The control of the desired tracking is represented in such a maneuver as turning the catamaran at different angles. The designed control system has shown good quality in terms of accuracy in tracking the desired heading angles**.**

Key-Words: - adaptive control, computational modeling, computer simulation, dynamics, kinematics, marine vehicles, mathematical model, nonlinear systems, numerical methods, system analysis and design.

Received: April 19, 2023. Revised: February 15, 2024. Accepted: March 23, 2024. Published: May 9, 2024.

1 Introduction

Unmanned autonomous vehicles are becoming increasingly important in both cyber-physical systems, Industry 4.0, and the whole global economy, [1]. These vehicles cannot be developed and operated without reliable mathematical models to replace the mental models existing in the heads of vehicles' human drivers, [2].

At Tallinn University of Technology (TalTech), one of the highest priority areas of study has been the research on catamaran sailboats. The control structures for autonomous sailboat navigation by using conventional or adaptive PID controllers were presented in [3]. Sail control was used to reduce heel and roll angles. The sail angle was optimized, whereas the rudder angle was controlled depending on the specified wind direction and the desired torque. The main goal was to ensure the long-term autonomous operation of sailing catamarans.

Recently, a new activity at TalTech has become the development of an electric catamaran called Nymo, an autonomous surface vehicle (ASV) for unmanned cargo transportation and environment monitoring purposes. Figure 1 shows the catamaran "Nymo" with a weight of 200 kg, a load capacity of up to 100 kg, and a possible distance of over 50 km.

Fig. 1: Catamaran "Nymo"

In this article, we model and simulate an ASV that corresponds to the catamaran "Nymo" in Figure 1. It is expected that the research results will be suitable for further development of real ASV and improvement of its control in harsh environmental conditions.

Here we offer and simulate a specially designed control system that effectively takes into account and adjusts the desired parameters like transition times, heading angle overshoot values, and the ratio of

coordinate-to-acceleration transition times for excellent performance at different heading angles stabilization tasks for ASV.

2 Model of Catamaran

Let us look at the catamaran model in Figure 2. This catamaran type of ASV has two separate hulls with separate propellers, where F_l and F_r are the port (left) and starboard (right) forces, respectively, which are provided by different thrusts; and d is the side hull separation. Figure 2 shows the definitions of the control system variables, where the heading angle ψ represents the orientation of the fixed frame of the ASV's body relative to the northeast-down frame. For convenience, the instantaneous ASV's heading angle φ is measured in an anticlockwise direction from the global X-direction. Then the angle φ is related to the heading angle by the next relation $\varphi = \frac{\pi}{2} - \psi$.

From Figure it can be seen that the control of the catamaran is based on the difference in the thrusts of the left and right propellers. If $F_l = F_r$, then the catamaran will move in a straight line. If $F_l \neq F_r$, it will cause a heading change in the catamaran because the difference in thrust forces between the two stern motors provides the turning moment.

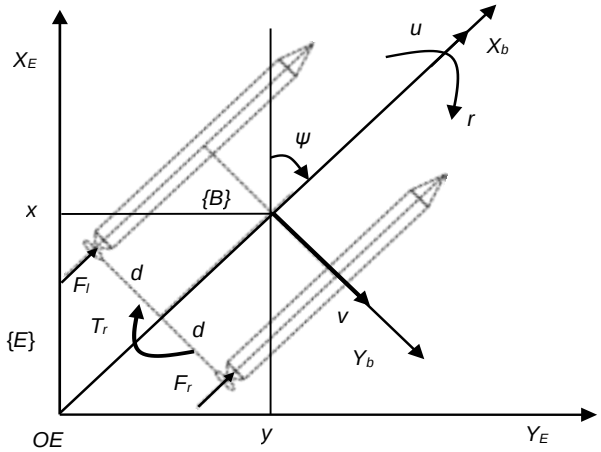

Fig. 2: Planar model of catamaran

The purpose is to capture the boat dynamics and be able to control the trajectory, thereby ensuring that the catamaran moves to the desired target angle as fast and safely as possible.

The kinematics of this control system can be presented as [4]:

$$\begin{bmatrix} \dot{x} \\ \dot{y} \\ \dot{\varphi} \end{bmatrix} = \begin{bmatrix} cos\,\varphi & -sin\,\varphi & 0 \\ sin\,\varphi & cos\,\varphi & 0 \\ 0 & 0 & 1 \end{bmatrix} \begin{bmatrix} u \\ v \\ r \end{bmatrix}, \quad (1)$$

where (x,y) denote the coordinates of the catamaran's center of mass in the Earth's coordinate system, φ is the ASV's heading angle; and u, v, r are the velocities of surge, sway, and yaw, respectively.

The system dynamics of the considered simplified mechanical model of the catamaran can be described using the next equations, [5]:

$$\begin{aligned} &m\dot{u} + m_{11}\dot{u} - mvr = F_x \\ &m\dot{v} + m_{22}\dot{v} + mur = F_y \\ &I_{zz}\dot{r} + m_{66}\dot{r} = N \end{aligned} \quad (2)$$

where m is the catamaran mass; m_{11}, m_{22}, m_{66} are the hull added masses; I_{zz} is the moment inertia of the catamaran in Z-direction; F_x, F_y, N are the external force in the X-direction, external force in Y-direction and external moment, respectively.

The external forces and moment in (2) can be defined as [6]:

$$\begin{aligned} &F_x = (1 - t_P)(F_r + F_l) \\ &F_y = 0 \\ &N = (1 + d_{NP})(F_r - F_l)d \end{aligned} \quad (3)$$

where t_P is the thrust deduction factor generated by the propeller in X-direction; d_{NP} is the propeller influence factor to the Y and Z-directions.

Note that in (3) no propeller forces are generated in the Y-direction.

The propeller's thrusts in (3) are defined as [7]:

$$\begin{aligned} &F_l = k_{tl}(J_{pl})\rho n_l^2 d_{pl}^4 \\ &F_r = k_{tr}(J_{pr})\rho n_r^2 d_{pr}^4 \end{aligned} \quad (4)$$

where k_{tl} and k_{tr} are the propeller's thrust coefficient functions of the left and right propellers, respectively; J_{pl} and J_{pr} represent the propeller's advance speed coefficients of the left and right propellers, respectively; ρ is the seawater density; n_l and n_r are the numbers of revolutions of the left and right propellers, respectively; d_{pl} and d_{pr} are the diameters of the left and right propellers, respectively.

Next, the coordinates of the center of mass and heading angle are obtained by the integration

$$\begin{aligned} &x(\tau) = \int_0^\tau \dot{x}(t)\,dt, y(\tau) = \int_0^\tau \dot{y}(t)\,dt, \\ &\varphi(\tau) = \int_0^\tau \dot{\varphi}(t)\,dt, \end{aligned} \quad (5)$$

where initial state $x(0) = 0, y(0) = 0, \varphi(0) = 0$.

From (1)-(5) it is clear that the position coordinates and heading angle of the ASV can be computed based on a given set of equations, desired target angle, and initial conditions.

3 Parameters of Catamaran

In this section, the ASV's parameters, [8], will be evaluated for the catamaran.

The next parameters of the control system can be obtained by direct measurements, [9]:

$$m = 225\ kg, d = 0.405\ m, d_p = 0.18\ m, l_x = 2.56\ m, l_y = 1.08\ m, l_d = 0.36\ m \quad (6)$$

where l_x, l_y, l_d are catamaran length, width, and draught, respectively.

The values of t_P and d_{NP} from (3) can be estimated as, [6]:

$$t_P = 0.25, d_{NP} = 0.25$$

The moment of inertia I_{zz} about the z-axis is calculated as [10]:

$$I_{zz} = \frac{m}{12}\left(l_x^2 + l_y^2\right) \quad (7)$$

Hence, from (6)-(7), we find:

$$I_{zz} = 144.7500\ kgm^2 \quad (8)$$

The hull-added masses from (2) are associated with the parameters of (6) and (8) as [5]

$$m_{11} = \frac{l_d m}{2l_x},$$
$$m_{22} = \frac{2l_d m}{l_y}\left(1 - \frac{l_y}{2l_x}\right)$$
$$m_{66} = \frac{2l_d I_{zz}}{l_y}\left(1 - \frac{1.6l_y}{l_x}\right) \quad (9)$$

Hence, the parameters in (9) have the following values:

$$m_{11} = 15.8203\ kg, m_{22} = 118.3594\ kg,$$
$$m_{66} = 31.3625\ kgm^2$$

It was known that a parameter ρ in (4) has the following value:

$$\rho = 1000\frac{kg}{m^3}$$

Let us now evaluate the value of F from (4) for one of the propellers.

The advance speed coefficient J_p from (4) for the selected propeller can be expressed as [11]

$$J_p = \frac{u}{nd_p} \quad (10)$$

where u is the surge velocity; n is the number of revolutions of the propeller; d_p is the diameter of the propeller.

For simulation, the propeller thrust coefficient function k_t will be approximated by a quadratic polynomial of J_p as follows:

$$k_t = a_1 J_p^2 + a_2 \quad (11)$$

where a_1, a_2 are the constant polynomial coefficients.

These polynomial coefficients in (11) can be obtained from the next linear equations:

$$a_1 J_{p1}^2 + a_2 = k_{t1}$$
$$a_1 J_{p2}^2 + a_2 = k_{t2} \quad (12)$$

Alternatively, equations (12) can be written in the form of a matrix so that:

$$WA_t = K_t \quad (13)$$

where

$$W = \begin{bmatrix} J_{p1}^2 & 1 \\ J_{p2}^2 & 1 \end{bmatrix}, A_t = \begin{bmatrix} a_1 \\ a_2 \end{bmatrix}, K_t = \begin{bmatrix} k_{t1} \\ k_{t2} \end{bmatrix}$$

The vector of polynomial coefficients from (13) can be expressed as:

$$A_t = W^{-1}K_t$$

Using the experimental data, [12]

$$u_1 = 0.4450\frac{m}{s}, u_2 = 0.8000\frac{m}{s},$$
$$n_1 = 400rpm, n_2 = 800rpm,$$
$$k_{t1} = 0.4104, k_{t2} = 0.3954$$

we find

$$A_t = \begin{bmatrix} 0.5699 \\ 0.3321 \end{bmatrix}$$

Combining (4), (10) and (11), we obtain that the value of propeller thrust can be estimated as:

$$F = \rho d_p^2\left(a_1 u^2 + a_2 d_p^2 n^2\right) \quad (14)$$

Then from (14), it follows that the number of revolutions can be calculated as follows:

$$n = \sqrt{\frac{F - a_1 \rho d_p^2 u^2}{a_2 \rho d_p^4}}$$

4 Control System

The thrust of the left propeller F_l can be considered as a fixed constant. Hence, we have

$$F_l = const \quad (15)$$

By choosing (15), the complex control problem now becomes a control problem using the starboard rotor thrust F_r as an input to control the heading angle φ.

The control system configuration for regulating the value of F_r r is then designed to have the structure shown in Figure 4.

$$\dot{F}_r = K_1(t_{11}(\varphi^0 - \varphi) - t_{21}\dot{\varphi} - \ddot{\varphi}) \quad (16)$$

where K_1, t_{11}, t_{21} are constants to be determined.

The variable F_r can be thought of as a "fast" function of time. Hence, assuming that $\dot{F}_r \approx 0$, from (16), we find

$$\ddot{\varphi} + t_{21}\dot{\varphi} + t_{11}\varphi = t_{11}\varphi^0 \quad (17)$$

The following coefficients in (17) are obtained for not exceeding the value of $\sigma \approx 5\%$, [13]

$$t_{11} \approx \frac{9}{t^2{}_{d_\varphi}}, t_{21} \approx \frac{3\sqrt{2}}{t_{d_\varphi}} \quad (18)$$

where t_{d_φ} is the desired transition time of φ.

From (1), we get

$$\dot{\varphi}(t) = r(t) \quad (19)$$

From (19), (2) and (3), we obtain

$$\ddot{\varphi}(t) = \frac{(1+d_{NP})F_r(t)d-(1+d_{NP})F_l(t)d}{I_{zz}+m_{66}} \quad (20)$$

From (20) and (15), we obtain

$$\ddot{\varphi}(t) = b(t)\dot{F}_r(t) \quad (21)$$

where

$$b = \frac{(1+d_{NP})d}{I_{zz}+m_{66}}. \quad (22)$$

Next, by combining (16) with (21), we obtain

$$\ddot{\varphi}(t) = bK_1(i_3(t) - \ddot{\varphi}(t)), \quad (23)$$

where

$$i_3(t) = t_{11}(\varphi^0 - \varphi(t)) - t_{21}\dot{\varphi}(t). \quad (24)$$

Defining $\ddot{\varphi}(t) = a(t)$ as in (23), we obtain

$$\dot{a}(t) = bK_1 i_3(t) - bK_1 a(t) \quad (25)$$

The variable $a(t)$ in (25) can usually be described using the following expression, [14]

$$a(t) = (a_0 + \int_0^t e^{-A(\tau)}bK_1 i_3(\tau)d\tau)e^{A(t)}, \quad (26)$$

where

$$A(t) = -\int_0^t bK_1 d\tau. \quad (27)$$

Let us now consider the behavior of the control system (Figure 4) over the time interval $t \geq t_{d\varphi}$ in a steady state.

Provided that $a_0 = 0$, $\varphi^0 - \varphi(t) \approx \Delta\varphi^0$, $\Delta = 0.05$, $\dot{\varphi}(t) \approx 0$, from (26)-(27), we find

$$a(t) = i_3(1 - e^{-bK_1 t}) \quad (28)$$

where

$$i_3(t) \approx t_{11}\Delta\varphi^0 = const. \quad (29)$$

The desired transition time for acceleration control lies in the overshoot zone with a value of σ≈5%. Then from (28), it follows that

$$t_{d\psi} = -\frac{ln(\Delta)}{bK_1} \quad (30)$$

Therefore, using (22) and (30), and assuming that $ln(\Delta) \approx -3$ and the ratio of coordinate-to-acceleration transition times $N_1 = \frac{t_{d_\varphi}}{t_{d\ddot{\varphi}}}$, we get

$$K_1 \approx \frac{3N_1(I_{zz}+m_{66})}{t_{d_\varphi}(1+d_{NP})d} \quad (31)$$

We can see from (18) and (31) that the coefficients K_1, t_{11}, t_{21} of the designed control system can be computed for a given equation (16) of control structure.

5 Simulation Results

The developed control system is used to control the approaching trajectory with a given heading angle at a constant number of revolutions of the left propeller $n_l = 200\ rpm$.

Simulation results for the proposed block diagram in Figure 3 (Appendix) are shown in Figure 5, Figure 6, Figure 7, Figure 8, Figure 9, Figure 10, Figure 11, Figure 12, Figure 13, Figure 14, Figure 15, Figure 16, Figure 17, Figure 18 and Figure 19 for various desired heading angles.

Note that different values were used for the ratio of coordinate-to-acceleration transition times ratio N_1 and desired transition time t_{d_φ} in (31) for different heading angles during those maneuvers.

The block diagram of the designed control system in Simulink is shown in Figure 4. The input signals as numbers of revolutions of the right propeller n_r are shown in Figure 5, Figure 8, Figure 11, Figure 14, and Figure 17. The output signals as heading angles φ are shown in Figure 6, Figure 9, Figure 12, Figure 15 and Figure 18. The trajectories of this ASV are shown in Figure 7, Figure 10, Figure 13, Figure 16 and Figure 19.

The different values for the heading angles are chosen for the simulations shown in Figure 5, Figure 6, Figure 7, Figure 8, Figure 9, Figure 10, Figure 11, Figure 12, Figure 13, Figure 14, Figure 15, Figure 16, Figure 17, Figure 18 and Figure 19. They are $\varphi_d = 45^0, 90^0, 135^0$, and 270^0, respectively.

Note that a very fast transition to the desired heading angles with high accuracy of regulation for those simulations was achieved.

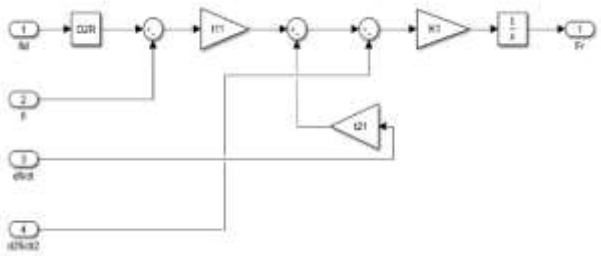

Fig. 4: Block scheme of the control system

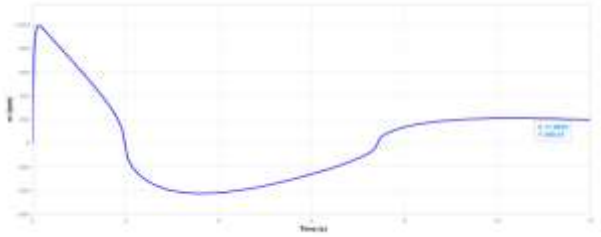

Fig. 5: Input signal of ASV for $\varphi_d = 45^0$

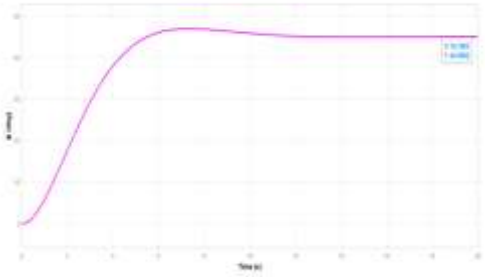

Fig. 6: Output signal of ASV for $\varphi_d = 45^0$

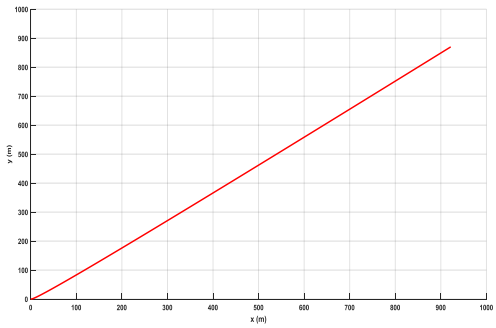

Fig. 7: ASV's trajectory for $\varphi_d = 45^0$, $N_1 = 50, t_{d\varphi} = 5\ s$ and stop time $t_{max} = 300\ s$

Fig. 8: Input signal of ASV for $\varphi_d = 90^0$

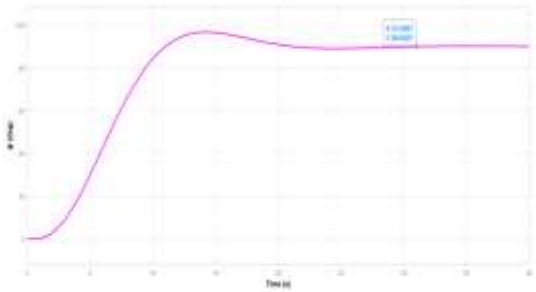

Fig. 9: Output signal of ASV for $\varphi_d = 90^0$

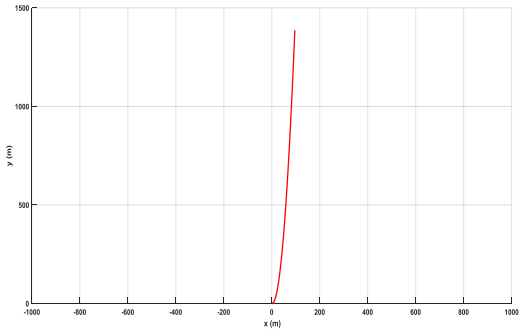

Fig. 10: ASV's trajectory for $\varphi_d = 90^0$, $N_1 = 3$, $t_{d\varphi} = 12\ s$ and stop time $t_{max} = 320\ s$

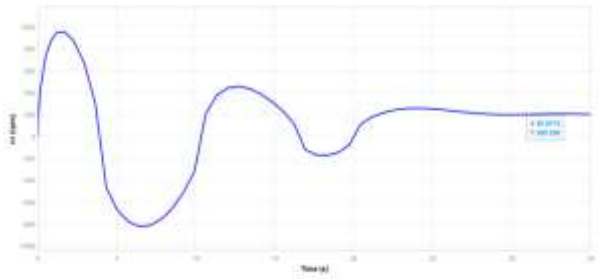

Fig. 11: Input signal of ASV for $\varphi_d = 135^0$

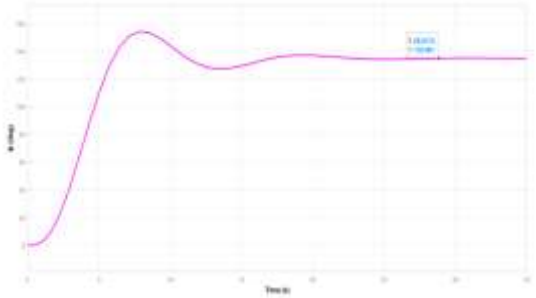

Fig. 12: Output signal of ASV for $\varphi_d = 135^0$

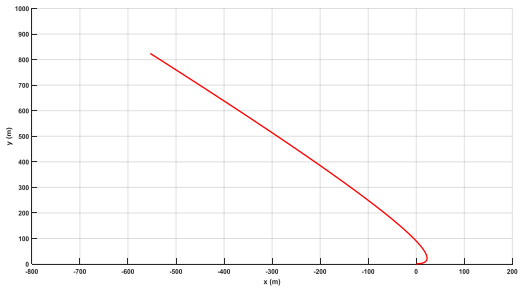

Fig. 13: ASV's trajectory for $\varphi_d = 135^0$, $N_1 = 2, t_{d_\varphi} = 7\ s$ and stop time $t_{max} = 290\ s$

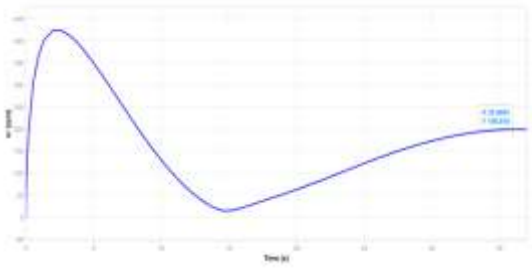

Fig. 14: Input signal of ASV for $\varphi_d = 180^0$

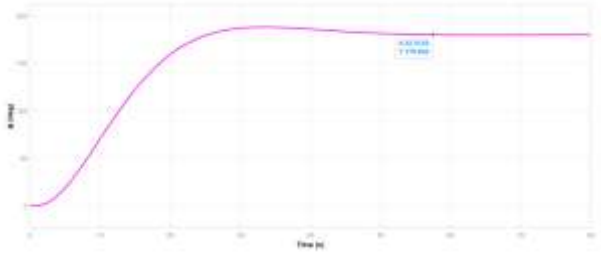

Fig. 15: Output signal of ASV for $\varphi_d = 180^0$

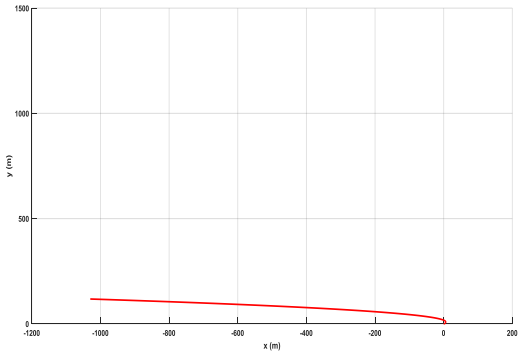

Fig. 16: ASV's trajectory for $\varphi_d = 180^0$, $N_1 = 8$, $t_{d_\varphi} = 24\ s$ and stop time $t_{max} = 310\ s$

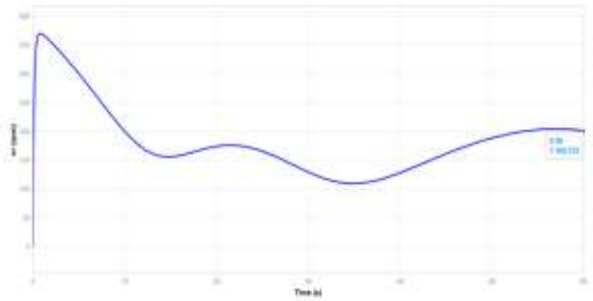

Fig. 17: Input signal of ASV for $\varphi_d = 270^0$

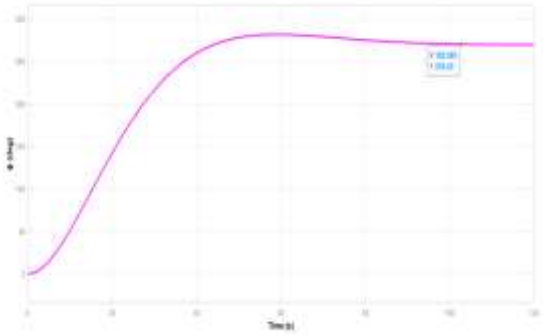

Fig. 18: Output signal of ASV for $\varphi_d = 270^0$

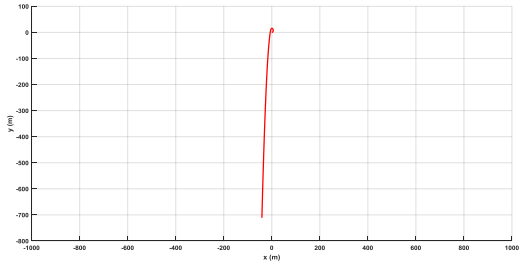

Fig. 19: ASV's trajectory for $\varphi_d = 270^0$, $N_1 = 75, t_{d_\varphi} = 40\ s$ and stop time $t_{max} = 280\ s$

Furthermore, the errors of regulation for the chosen heading angles were significantly less than the waited value of 5%. They are -4e-3%, -7e-4 %, 4e-4 %, -3e-4%, and 1e-4 %, respectively.

6 Conclusions

The modeling and simulation techniques have been presented and analyzed for the real autonomous electric catamaran "Nymo" in the Simulink/MATLAB environment. These techniques enable adjustment of the desired parameters like transition times, heading angle overshoot values, and the ratio of coordinate-to-acceleration transition times for performing such maneuvers as the turn of the catamaran at different angles.

The proposed controller design methodology can be used to improve the ASV's model design for

various applications, including various reliable positioning monitoring tasks. From the application point of view, the methodology provides a valuable practical opportunity to improve the motion characteristics of the catamaran "Nymo" dedicated to environment monitoring and cargo transporting under difficult sea conditions. In addition, the designed control system with relatively simple realization can be easily applied to other types of ASVs.

The simulation results have confirmed the impressive quality of the offered optimal nonlinear control approach to assure the smooth and fast stabilization of ASV's trajectories.

Acknowledgment:
Research for this publication was funded by the EU Horizon2020 project 952360-MariCybERA.

References:

[1] V. Tsiatsis, S. Karnouskos, J. Holler, D. Boyle, and C. Mulligan, "Autonomous vehicles and systems of cyber-physical systems," in *Internet of Things: Technologies and Applications for a New Age of Intelligence*, London: Academic Press, 2019, pp. 299–305, DOI:10.1016/B978-0-12-814435-0.00029-8.

[2] M. R. Endsley, "Toward a theory of situation awareness in dynamic systems," *Human Factors*, Vol. 37, Issue 1, 1995, pp. 32–64, DOI:10.1518/001872095779049543.

[3] I. Astrov, A. Udal, H. Mõlder, T. Jalakas, and T. Möller, "Wind force model and adaptive control of catamaran model sailboat," Proc**.** *IEEE 8th Int. Conference on Automation, Robotics and Applications***,** *ICARA 2022*, Prague, Czech Republic, pp. 202–208, 2022, DOI:10.1109/ICARA55094.2022.9738524.

[4] M. J. Hong and M. R. Arshad, "Modeling and motion control of a riverine autonomous surface vehicle (ASV) with differential thrust," *Jurnal Teknologi (Sciences & Engineering)*, Vol. 74, Issue 9, 2015, pp. 137−143, DOI:10.11113/jt.v74.4817.

[5] V. Ferrari, S. Sutulo, and C. Guedes Soares, "Preliminary investigation on automatic berthing of waterjet catamaran" in *Maritime Engineering and Technology*, C. Guedes Soares and T. A. Santos, (eds.), London: Taylor & Francis Group, 2015, pp. 1105–1111, DOI:10.13140/2.1.2551.0725.

[6] J. Pandey and K. Hasegawa, "Path following of underactuated catamaran surface vessel (WAM-V) using fuzzy waypoint guidance algorithm," Proc. *IEEE SAI Intelligent Systems Conference, IntelliSys 2016*, London, UK, pp. 995–1000, 2016, DOI:10.1007/978-3-319-56991-8_45.

[7] Propeller thrust, [Online]. https://www.sciencedirect.com/topics/engineering/propeller-thrust (Accessed Date: February 8, 2024).

[8] Nymo shows the future of maritime industry, [Online]. https://researchinestonia.eu (Accessed Date: February 8, 2024).

[9] Nymo technical parameters, [Online]. Available from: https://mindchip.ee/nymo/ (Accessed Date: February 8, 2024).

[10] Parallelepiped rotating around its central axis, [Online]. http://www.claredot.net/en/sec-MomMasInertia/Mom_11.php (Accessed Date: February 8, 2024).

[11] Advance Coefficient, [Online]. https://www.sciencedirect.com/topics/engineering/advance-coefficient (Accessed Date: February 8, 2024).

[12] Model Test Report 0015-1 "2.5 m Autonomous Surface Vessel", [Online]. https://www.scc.ee/asv-platform-and-manoeuvring-test-development-2018-2019/ (Accessed Date: February 8, 2024).

[13] P. D. Krutko, *Inverse Problems of Control System Dynamics: Nonlinear Models*. Moscow: Nauka, 1989.

[14] L. S. Pontryagin, *Ordinary Differential Equations*. Moscow: Nauka, 1974.

APPENDIX

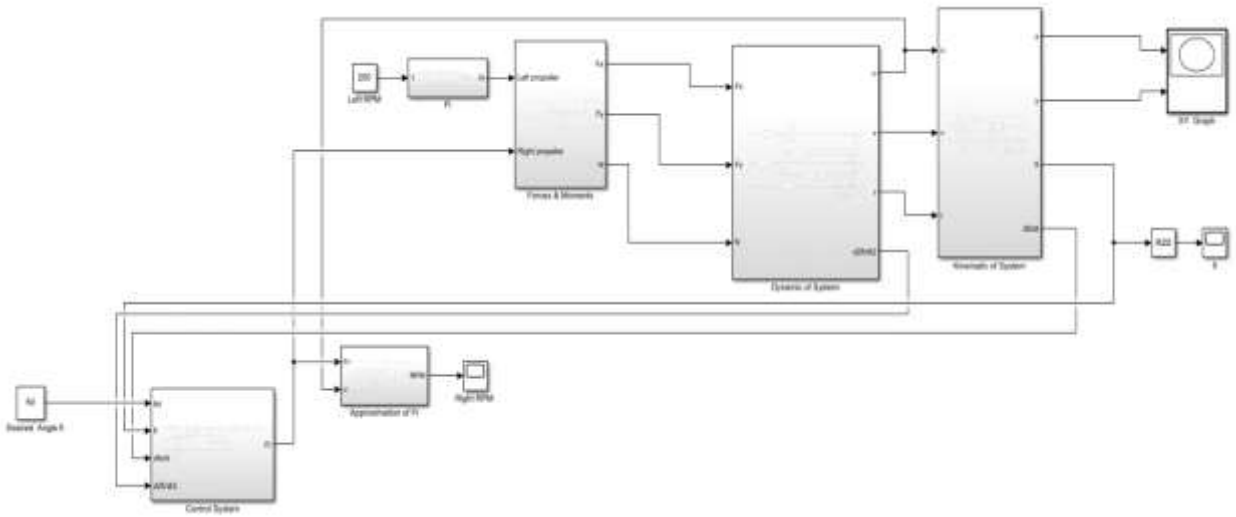

Fig. 3: Block diagram of ASV

Contribution of Individual Authors to the Creation of a Scientific Article (Ghostwriting Policy)
The authors equally contributed to the creation of this article at all stages from problem formulation to final findings and solution.

Sources of Funding for Research Presented in a Scientific Article or Scientific Article Itself
This article was funded by the EU Horizon 2020 project MariCybERA, agreement No. 952360.

Conflict of Interest
The authors have no conflicts of interest to declare.